Petroleum Science 23 (2026) 7155–7168

Contents lists available at ScienceDirect

Petroleum Science

journal homepage: www.keaipublishing.com/en/journals/petroleum-science

Original Paper

Hydrocarbon evaporation behavior in medium-to high-maturity shale: Insights from pressure-retained core samples

Ming Li [a,b], Yan Wu [b,*], Li Fu [c,d], Min Wang [b,**], Xue Wang [c,d], Jin-Bu Li [e], Liang Xu [c,d], Yong-He Sun [a], Xin-Bin Zhao [b], Shang-De Dong [b]

[a] Chongqing Unconventional Oil and Gas Development Research Institute, Chongqing University of Science and Technology, Chongqing, 401331, China
[b] State Key Laboratory of Deep Oil and Gas, China University of Petroleum (East China), Qingdao, 266580, Shandong, China
[c] Exploration and Development Research Institute, Daqing Oilfield Company Ltd., PetroChina, Daqing, 163712, Heilongjiang, China
[d] National Key Laboratory for Multi-resource Collaborated Green Development of Continental Shale Oil, Daqing, 163712, Heilongjiang, China
[e] Guangzhou Institute of Geochemistry, Chinese Academy of Sciences, Guangzhou, 510640, Guandong, China

ARTICLE INFO

Article history:
Received 14 September 2025
Received in revised form
1 January 2026
Accepted 8 May 2026
Available online 13 May 2026

Edited by Min Li

Keywords:
Hydrocarbon evaporation
Shale oil composition
Medium-to high-maturity shale
Pressure-retained core

ABSTRACT

Focusing on the medium-to high-maturity shale oil play of the Qingshankou Formation in the Gulong Sag (Songliao Basin, NW China), pressure-retained, full-closure, and conventional core samples (including long-term stored core samples) with varying thermal maturities were collected, to visually demonstrate the changes in oil content and retained hydrocarbon composition during exposure. The factors influencing the evaporative loss of light hydrocarbons were investigated. We utilized T_1-T_2 nuclear magnetic resonance (T_1-T_2 NMR), thermal desorption-gas chromatograph (TD-GC) and Rock-Eval analysis techniques to examine pressure-retained core samples during exposure. A fitting formula was established to describe the relationship between oil content and exposure time. The evaporation of oil content in sample H1-1 (R_o = 1.55%) was best modeled using a power-law decay, whereas an exponential decay provided a better fit for the samples B5-1 (R_o = 1.20%) and G5-1 (R_o = 1.32%). The oil content detected by T_1-T_2 NMR was significantly higher than that obtained by TD-GC, with Rock-Eval analysis yielding the lowest values. During the exposure of pressure-retained core samples, nearly all nC_{9-} alkanes were lost, $nC_{10–14}$ showed substantial loss, and nC_{15+} alkanes experienced partial evaporation in higher maturity samples. Thermal maturity controls the evaporative loss of light hydrocarbons in shale, as reflected in oil composition and pore structure. In high maturity shale, organic matter has minimal impact on hydrocarbon loss, while variations in mineral composition often lead to changes in pore structure. The evaporation rate of block samples is lower than that of powdered samples, with smaller particle sizes exhibiting faster loss rate. Higher temperatures and lower humidity in storage facilitate hydrocarbon diffusion. The research enhances the understanding of light hydrocarbon evaporation processes and offers new insights for evaluating in situ oil content and composition.
© 2026 The Authors. Publishing services by Elsevier B.V. on behalf of KeAi Communications Co. Ltd. This is an open access article under the CC BY-NC-ND license (http://creativecommons.org/licenses/by-nc-nd/4.0/).

1. Introduction

The thermal maturity of shale, typically quantified by vitrinite reflectance (R_o), plays a crucial role in controlling various characteristics, including pore structure, oil content, shale oil composition, enrichment pattern, phase behavior and transport of fluids under confinement. Shale oil is classified into two categories: low- to medium-maturity shale oil (0.5% < R_o < 0.9%) and medium-to high-maturity shale oil (R_o ≥ 0.9%, with an optimal range of 1.0%–1.6%) (Zhao et al., 2020, 2023a). Medium-to high-maturity shale oil plays exhibit significant potential due to high proportion of gaseous hydrocarbons, low crude oil density, and overpressured fluids (Hu et al., 2022; Sun et al., 2023; Zhao et al., 2023b). Shale oil has become a key resource supporting stable crude oil production in China.

Experimental analysis based on core samples remains the most reliable and convincing method for obtaining the properties of shale, including shale oil. However, due to the high proportion of light hydrocarbons in medium-to high-maturity shale oil, and the

* Corresponding author.
** Corresponding author.
E-mail addresses: B22010079@s.upc.edu.cn (Y. Wu), wangm@upc.edu.cn (M. Wang).
Peer review under the responsibility of China University of Petroleum (Beijing).

https://doi.org/10.1016/j.petsci.2026.05.010
1995-8226/© 2026 The Authors. Publishing services by Elsevier B.V. on behalf of KeAi Communications Co. Ltd. This is an open access article under the CC BY-NC-ND license (http://creativecommons.org/licenses/by-nc-nd/4.0/).

sharp drop in temperature and pressure during coring, a large amount of light hydrocarbons (C_1–C_9) are lost (Mango, 1997; Cañipa-Morales et al., 2003; Sun et al., 2013; Jiang et al., 2016). Furthermore, long-term storage and pre-preparation (such as cutting and crushing) exacerbate hydrocarbon evaporative loss. Although the loss of hydrocarbons has long been a focus of scholarly attention, most research has primarily emphasized changes in the composition of bulk fluids under ambient conditions. Fingas reviewed the physics and mathematical modeling of oil spill evaporation (Fingas, 1995), and studied the time-dependent evaporation of several crude oils and petroleum products (Fingas, 1997, 1998). Cañipa-Morales et al. (2003) reported on the impact of partial evaporation on C_7 light hydrocarbon parameters, demonstrating that preserving crude oils from evaporation is essential for accurate application of all light hydrocarbon parameters. Okamoto et al. (2010) developed a prediction model for the variation in the composition of multi-component liquid phases during evaporation. Zhu et al. (2012) presented experimental analysis of the evaporation process for 93 RON unleaded gasoline. Xiao et al. (2012) used condensate samples from the Tarim Basin (NW China) to investigate the stable carbon isotopic fractionation of individual light hydrocarbons in the C_6–C_8 range. Similarly, Sun et al., 2013 conducted laboratory experiments on condensate oil from the Tarim Basin, investigating the effects of natural evaporation on C_5–C_8 light hydrocarbon indicators. Li et al. (2014) explored the effects of atmospheric evaporation on the concentration and distribution of low molecular weight diamondoids in four petroleum fractions (gasoline, condensate, diesel, and fuel oil). Liu et al. (2024) performed evaporation experiments at a constant temperature on light hydrocarbons in single compound, alkane mixture, and light oil, and assessed the contents and H isotopic compositions of individual light hydrocarbons in the residual liquid phase. However, the evaporation behavior of fluids in pores differs from that of bulk fluids. Evaporation of pore fluids occurs in two stages: the pore fluids first flow or diffuse to the sample surface, and then volatilizes from the surface. The properties of shale, especially minerals, organic material and pore structure, may have an impact on fluids evaporation.

Hydrocarbon loss not only results in an underestimation of oil content but also leads to a skewed understanding of retained hydrocarbon composition. While many scholars have recognized the impact of light hydrocarbons loss on oil content evaluation and proposed various recovery methods for Rock-Eval S_1 (Cooles et al., 1986; Wang et al., 2014, 2022a; Jarvie, 2014; Zhu et al., 2015; Jiang et al., 2016, Jiang et al., 2019; Chen et al., 2018), few have delved into the specific process of hydrocarbon evaporation. Jiang et al. (2016) characterized the changes in oil content and hydrocarbon composition over time in shale samples from the organic-rich Devonian Duvernay Formation (Western Canada Sedimentary Basin) and the organic-lean Ordovician Lotbinière Formation (St. Lawrence Platform, Quebec, Canada). The samples exhibited the loss of gaseous hydrocarbons and light hydrocarbons with a carbon number less than 10 after coring, preservation, and experimental pretreatment. They also found that the higher the organic matter content in the shale, the slower evaporative loss of light hydrocarbon due to stronger adsorption. However, the samples in the study had been stored at ambient conditions for 2 years and 6 months before being sent to the laboratory for geochemical analysis. Furthermore, Beti et al. (2020) presented a thermodynamic model to explain the changes in hydrocarbon composition of rock samples (Duvernay shale) over time while residing in a laboratory environment. Qian et al., 2022 selected fresh shale samples (R_o = ~0.9%) from the third member of Qianjiang Formation (Paleogene, Jianghan Basin, China) and conducted time-series experiments on the oil content and hydrocarbon composition of the samples varying placement times. The evaporative composition primarily consisted of low-carbon hydrocarbons, up to C_{13}–C_{15}, while medium to heavy compounds were less affected. Additionally, the study revealed that the extent and proportion of light hydrocarbons loss were closely related to the original oil content, porosity, and permeability. Although the samples used were frozen immediately and preserved at low temperatures (−40 °C) after coring, they were still obtained via conventional coring, where hydrocarbon loss is inevitable. Rock-Eval, thermal desorption-gas chromatograph (TD-GC), and T_1-T_2 nuclear magnetic resonance (T_1-T_2 NMR) analyses were conducted on high maturity shale samples from pressure-retained coring, offering a new approach and perspective for understanding hydrocarbon evaporation (Zeng et al., 2021; Li et al., 2022a, 2022b, 2024a).

To further elucidate the process of light hydrocarbons evaporation and influencing factors, this study selected a representative medium-to high-maturity shale oil play from the Gulong Sag, Songliao Basin, NW China. We focused on evaporative loss of light hydrocarbons by analyzing shale samples from pressure-retained coring and full-closure coring with varying maturities. Through Rock-Eval, TD-GC, T_1-T_2 NMR and conventional analyses, the evaporation process of light hydrocarbons was visually demonstrated, including changes in oil content and residual hydrocarbon composition, and the key factors affecting hydrocarbon evaporation were identified. The research provides valuable insights for evaluating oil content, determining in situ oil composition, and describing phase behavior of confined fluids in nanopores.

2. Geological setting

The Qijia–Gulong Sag is the primary oil-generating region of the Songliao Basin. The thick shales deposited in the Qingshankou Formation (99.6 ± 0.5 Ma to 88.5 ± 0.5 Ma, Upper Cretaceous) have generated oil and gas that migrated both downward and upward through faults and sand bodies, forming large-scale conventional and tight oil reservoirs, including Yangdachengzi, Fuyu, Gaotaizi, Putaohua, Sartu, and Heidimiao oil layers (He, 2023; Liu et al., 2023). The crude oil retained within the source rock has formed the Gulong shale oil play, particularly in the first member and the lower section of the second member of the Qingshankou Formation (the target interval). The interval is a representative example of continental medium-to high-maturity shale oil in China (Fig. 1(a)). Shale oil is predominantly distributed in the central and southern regions of the Qijia-Gulong Sag, referred to as the Gulong Sag. The favorable oil-producing sections of the Qingshankou Formation are stratigraphically divided into nine sub-layers (Q1–Q9) from bottom to top. Of these, Q1 to Q6 corresponds to the first member of the Qingshankou Formation (Mbr 1 of the Qingshankou Fm), while Q7 to Q9 belongs to the second member of the Qingshankou Formation (Mbr 2 of the Qingshankou Fm) (Fig. 1(b)).

The target interval consists of shale and mudstone interbedded with thin layers of siltstone, dolomite, and shell limestone. The thickness of single layer is typically less than 10 cm, with cumulative thickness accounting for less than 10% of the whole interval (Zhu et al., 2023). The shale oil play in the Qingshankou Formation (Q1–Q9) of the Gulong Sag is characterized by pronounced source–reservoir integration, resulting from an optimized configuration between hydrocarbon source rocks and storage space (Guo et al., 2025). The kerogen within the interval is primarily Type I, with locally Type II_1. The vitrinite reflectance (R_o) of kerogen in Mbr 1 of the Qingshankou Fm is generally greater than 0.9%, exceeding 1.2% in the core area (Sun et al., 2021; He et al., 2022; Wang et al., 2023). High maturity and elevated clay mineral

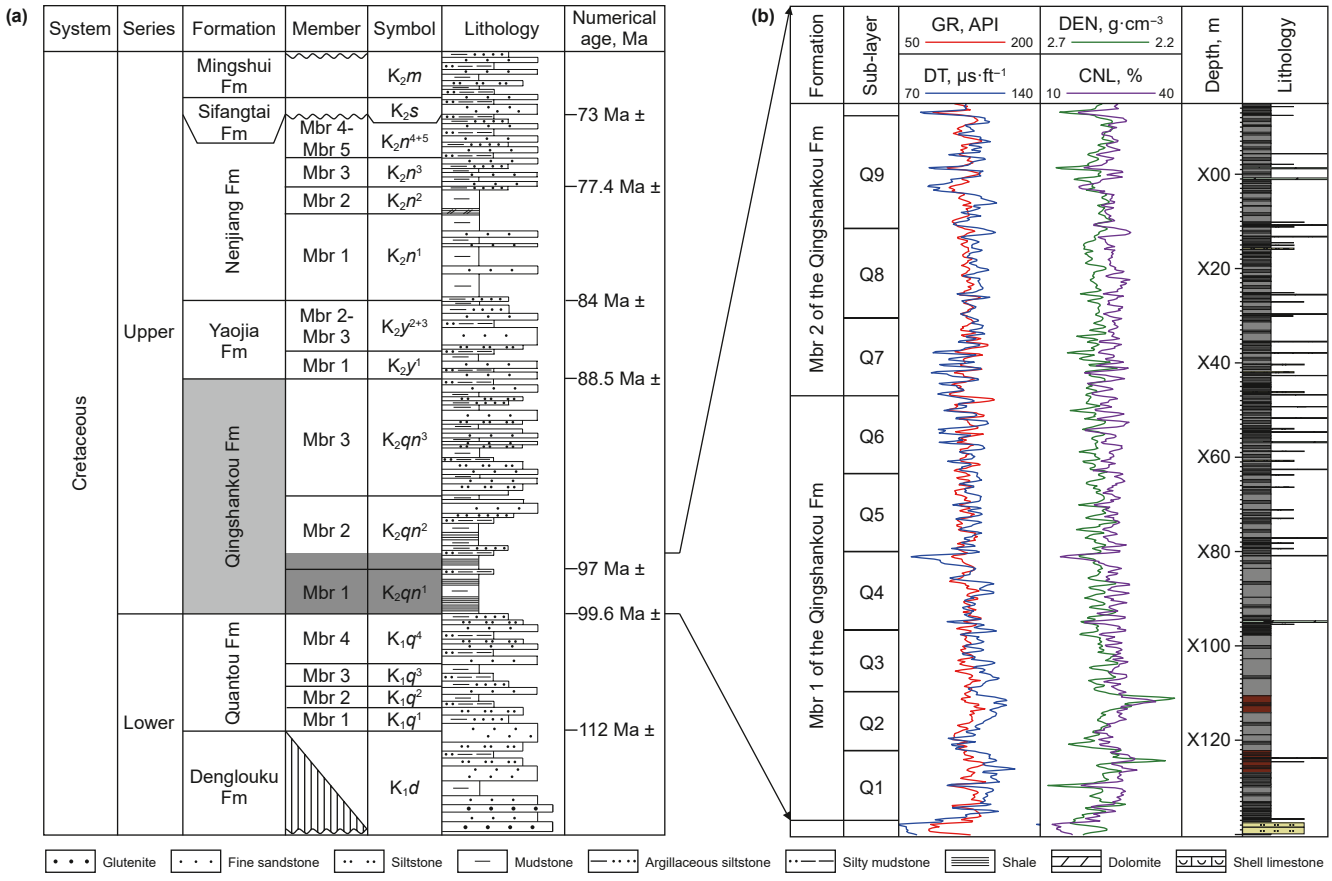


Fig. 1. Stratigraphic architecture in the target area. **(a)** Stratigraphic chart of the northern Songliao Basin (modified after He (2023)), **(b)** Q1–Q9 sub-layers in the Qingshankou Formation, H1 well in the Gulong Sag.

content (35 wt%–50 wt%) are key characteristics of the Qingshankou Fm in the Gulong shale oil play. As of August 2024, five "field laboratory" test sites and one expanded test site have been established in the region.

3. Samples and methods

The samples analyzed in the study were primarily sourced from the Q1–Q9 sub-layers and consisted of pressure-retained core samples, full-closure core samples, and conventional core samples (including long-term stored samples). Pressure-retained coring, which preserves cores at reservoir pressure conditions, is considered the most effective method for obtaining in situ fluid content and composition, particularly for high maturity shale oil play. Full-closure coring involves sealing the core with a sealing fluid to prevent fluid loss (American Petroleum Institute, 1998). The analyzed core samples exhibit thermal maturities (R_o) ranging from 0.90% to 1.55%. In total, 51 specimens were collected from 7 wells in the Gulong Sag, covering a depth interval of approximately 1900–2500 m, thereby ensuring representative coverage of the target stratigraphic interval. Pressure-retained cores and full-closure cores were cut into cubes using a blade in a liquid nitrogen-cooled environment and were immediately stored in liquid nitrogen tanks. Before the experiment, the samples were quickly retrieved from the liquid nitrogen tanks and divided into three parts. The cubes and pulverized samples were exposed to air at room temperature (about 22 °C) over durations that varied from 3 days to 2 weeks. Techniques such as T_1-T_2 NMR, TD-GC, and Rock-Eval were employed to obtain oil content and hydrocarbon composition (Fig. 2).

3.1. T_1-T_2 NMR

Nuclear magnetic resonance (NMR) technology offers significant advantages in studying fluid distribution in tight reservoirs, including rapid detection, non-destructive analysis, and the ability to simultaneously provide information on both pores and fluids (Fleury and Romero-Sarmiento, 2016; Liu et al., 2019; Song and Kausik, 2019; Zhang et al., 2020, 2024; Mukhametdinova et al., 2021). However, due to the extremely low temperature of samples retrieved from liquid nitrogen tanks, proton signals are suppressed, preventing fluid detection by NMR. Therefore, the frozen samples must be thawed prior to the NMR experiment. The thawing process is monitored by continuously measuring the T_2 NMR signal. When the total signal value stabilizes and no longer increases, the sample is considered fully thawed, allowing the T_1-T_2 NMR test to begin. After completing the test, the oil content of samples with varying exposed times was determined using T_1-T_2 NMR. The mass of the cube samples used in the T_1-T_2 NMR test ranges between 10 and 20 g.

A high-precision NMR core analyzer (MR Cores-XX), manufactured by CoreLab in the United States, was utilized in the research. The analyzer features a magnetic field strength of 0.5 T, a frequency of 22 MHz, a magnet temperature of 35 °C, and a probe diameter of 30 mm. The echo time (TE) and wait time (TW) are set at 0.07 and 1000 ms, respectively, with 4000 echoes recorded. The

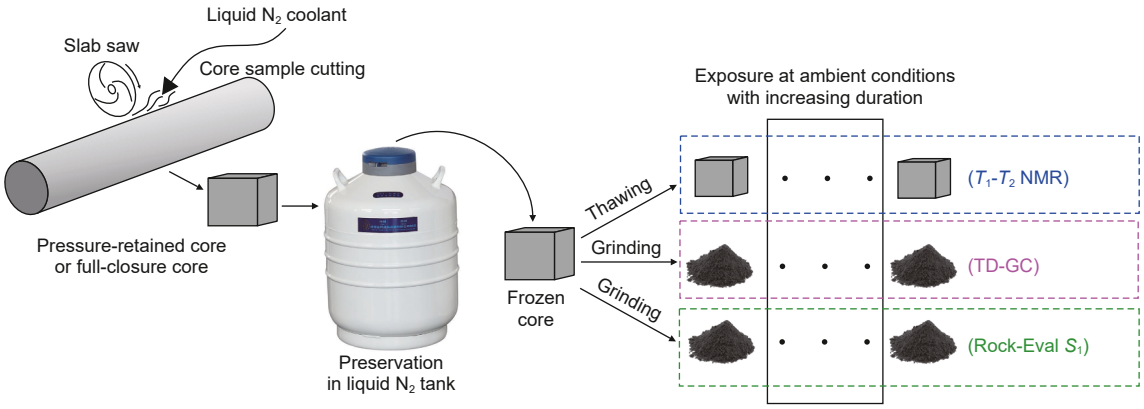


Fig. 2. Sample preparation and treatment for experiments.

instrument significantly reduces the signal acquisition dead time to 15 μs, enabling the detection of solid organic matter (kerogen) and fluids within nanopores. The duration of T_1-T_2 NMR test ranges from 5 to 10 min. The Carr-Purcell-Meiboom-Gill (CPMG) pulse sequence was employed to identify and quantify hydrogen-containing fluids in the samples. A fluid signal–mass equation was established by conducting T_2 NMR tests on shale oil from Mbr 1 of the Qingshankou Fm with varying maturity (Li et al., 2022b). For detailed information on the distribution of hydrogen-containing components of shale on the T_1-T_2 NMR map, please refer to the previous literatures published by our team (Li et al., 2018, 2019a, 2019b, 2024b).

3.2. TD-GC

TD-GC can not only detect the composition of oil trapped in the shale pores but also perform quantitative analysis. Take out the core stored in the liquid nitrogen tank and quickly grind it to 20–60 mesh, which takes 10–15 s. Weigh 30–50 mg of the pulverized sample and place it into the crucible. The powder was heated at 300 °C for 3 min to fingerprint the Rock-Eval S_1 equivalent of free hydrocarbons (Jiang et al., 2016). Hydrocarbons released from shale were first collected on a trapping media (liquid nitrogen), and were transferred via a high-fidelity heated transfer system to gas chromatography along with a carrier gas (helium). A Shimadzu GC-14B instrument (Japan) equipped with an HP-5 petroleum capillary column (50 m × 0.20 mm × 0.5 μm) (Li et al., 2024c).

3.3. Rock-Eval pyrolysis

Rock pyrolysis testing, including both routine and multi-step pyrolysis methods (Romero-Sarmiento et al., 2016a, 2016b, 2019; Wang et al., 2022), is one of the most widely applied and widely accepted approaches for estimating shale oil content. The core samples were removed from the liquid nitrogen tank and promptly grinded to a particle size of 60–80 mesh. Approximately 30 mg of the pulverized sample was then used for pyrolysis analysis. In the study, a Rock-Eval 6 pyrolysis instrument was utilized. The sample was heated at a constant temperature of 300 °C for 3 min to obtain pyrolysis S_1.

In addition to the three main experiments mentioned above, established techniques were also employed to determine the basic characteristics of the samples used, including total organic carbon (TOC) analysis, vitrinite reflectance (R_o) measurement, X-ray diffraction (XRD), nitrogen adsorption, and thin-section identification.

4. Results and discussions

4.1. Changes in oil content during exposure

4.1.1. Oil content detected by T_1-T_2 NMR

Due to the high maturity of Mbr 1 of the Qingshankou Fm in the Gulong Sag and relatively low TOC (TOC < 2.5%), the content of adsorbed oil is minimal (Li et al., 2023), which is evidenced by the near absence of signals in area E on the T_1-T_2 NMR map (Figs. 3 and 4). Compared to the free oil content, the adsorbed oil is negligible. Sample H1-1 was collected from Well H in the Q4 sub-layer of Mbr 1 of the Qingshankou Formation and exhibits a relatively high thermal maturity (R_o = 1.55%; Table S1). The NMR signals for sample H1-1 are primarily distributed in areas A, B, and C. The T_1-T_2 NMR maps of samples with increasing exposed time clearly showed that the signal in area A diminishes rapidly. After 1.46 h, almost no obvious signal was observed in area A, indicating a significant decrease in oil content for evaporative loss. Additionally, the signals in area B also decline, suggesting that free water evaporation occurs. However, the evaporation of pore water is not the focus of this study. By extracting the signal in area A, the oil content of shale at various exposure times was quantified using the signal-mass equation. For sample H1-1, the initial signal in area A was 1.59 pu, corresponding to an oil content of 13.35 mg/g. After 0.13 h (8 min), the signal in area A dropped to 0.75 pu, with an oil content of 7.05 mg/g, indicating that 52.83% of the crude oil had already evaporated. At 0.29 h (17 min), the signal decreased further to 0.69 pu. After 1.46 h (87 min), the signal fell to 0.63 pu, with the oil content reducing to 5.28 mg/g. At 5.44 h (327 min), the signal in area A was 0.51 pu, corresponding to an oil content of 4.31 mg/g, with 67.74% of the crude oil evaporated. After 24.4 h, the area A signal was 0.46 pu. Following 263.08 h (approximately 11 days), the signal dropped to 0.22 pu, with the oil content decreasing to 1.86 mg/g. After 435.32 h (about 18 days), the signal further decreased to 0.18 pu, corresponding to an oil content of 1.54 mg/g, with 88.49% of the crude oil evaporated (Fig. 3).

For sample G5-1, collected from Well G2 in Mbr 1 of the Qingshankou Fm (Q6 sub-layer) with slightly lower maturity (R_o = 1.32%) compared to sample H1-1 (Table S1), the initial signal in area A was 0.82 pu, corresponding to an oil content of 7.01 mg/g. After 0.33 h (20 min), the signal in area A dropped to 0.74 pu, with an oil content of 6.27 mg/g, indicating that 10.60% of the crude oil had evaporated. At 1.33 h (80 min), the signal further decreased to 0.66 pu, with an oil content of 5.65 mg/g. After 4.33 h (260 min), the signal fell to 0.55 pu, with an oil content of 4.68 mg/g, representing a loss of 33.29%. At 23.42 h (1405 min), the signal in area A declined to 0.43 pu, corresponding to an oil content of 3.64 mg/g.

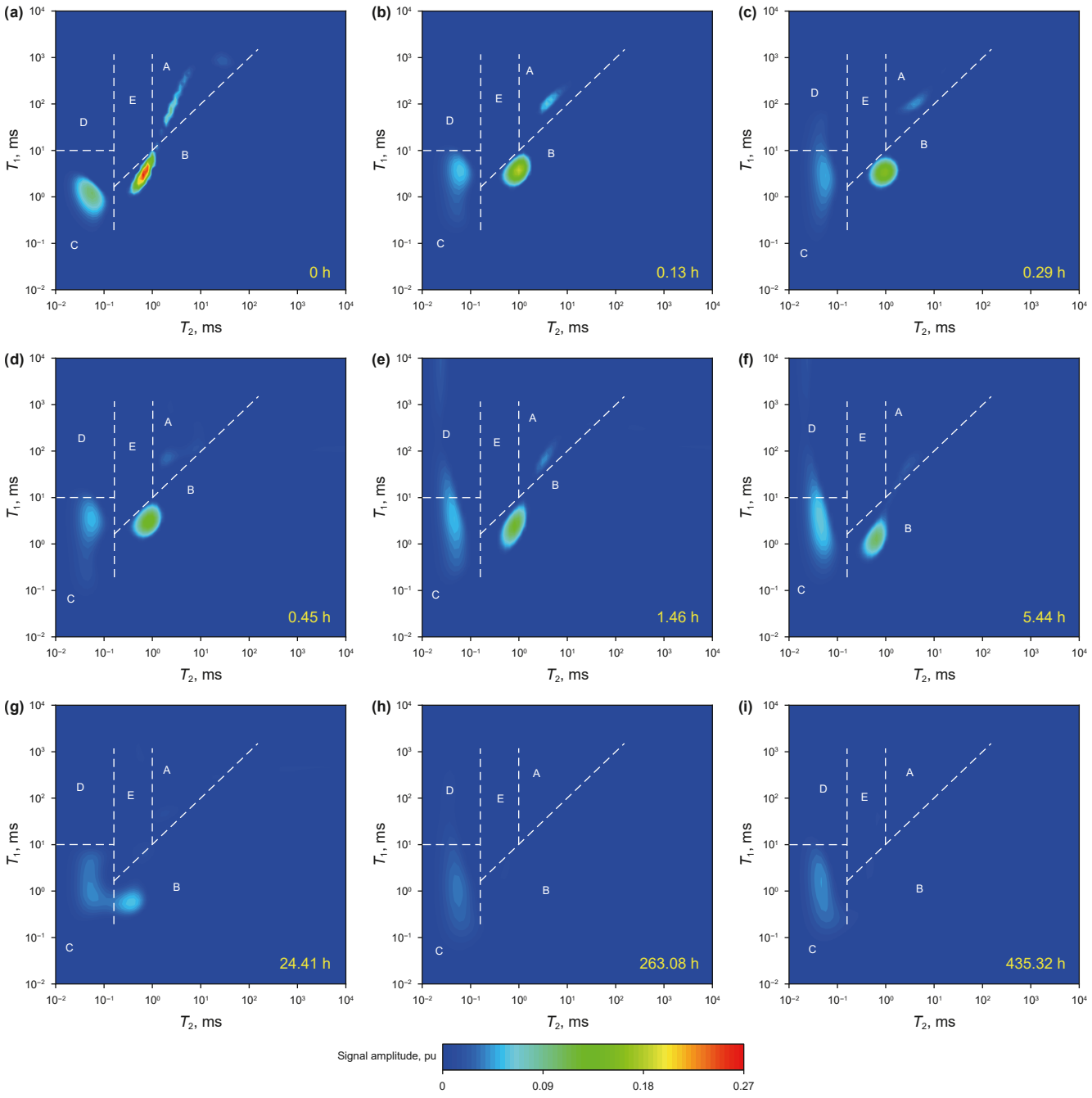


Fig. 3. T_1-T_2 NMR maps of sample H1-1 (R_o = 1.55%) at different time periods of exposure. Area A refers to free oil, area B refers to free water, area C refers to adsorbed and structural water, area D refers to kerogen and area E refers to adsorbed oil (Li et al., 2018).

After 151.57 h (just over 6 days), the signal in area A dropped significantly to 0.24 pu, with the oil content reducing to 2.08 mg/g. At this point, 70.35% of the crude oil had evaporated (Fig. 4).

4.1.2. Oil content detected by TD-GC

The initial oil content of sample H1-1, as determined by TD-GC, was 6.97 mg/g. After the pulverized sample was left for 2 min, the oil content decreased to 2.88 mg/g, resulting in a loss of 58.67% of the crude oil within a short time. After 20 min, the oil content further declined to 2.01 mg/g. At 20 h, the oil content measured 1.69 mg/g, corresponding to a loss rate of 75.73%. After 8 days, the oil content was 1.61 mg/g, with a total loss of 76.92%. For sample G5-1, the initial oil content was 3.10 mg/g. After 2 min, the oil content dropped to 2.12 mg/g, reflecting a loss of 31.77%. At 20 min, the oil content was 1.66 mg/g, with 46.50% of the crude oil evaporated. After 24 h, the oil content further decreased to 1.44 mg/g, with a loss rate of 53.68%. Beyond this point, the oil content stabilized with increasing storage time. After 6 days, the oil content measured 1.43 mg/g, indicating a total loss of 53.93% (Fig. 5).

4.1.3. Oil content detected by Rock-Eval pyrolysis

The initial Rock-Eval S_1 of sample H1-1 was 2.33 mg/g. After 2 min, the S_1 decreased to 1.71 mg/g. Subsequently, the S_1 declined in a fluctuating path. After 3 days, the S_1 dropped to 1.46 mg/g,

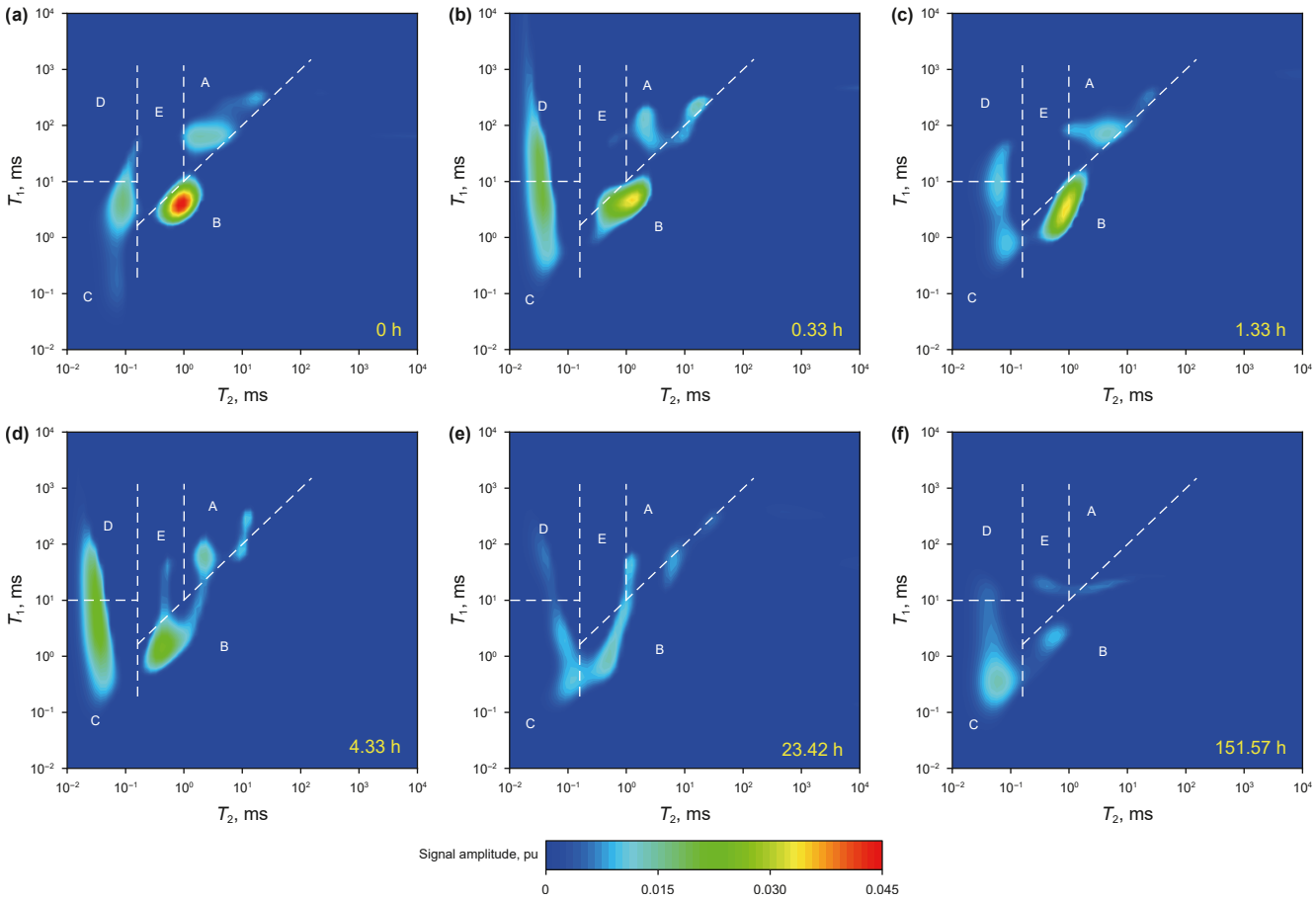


Fig. 4. T_1-T_2 NMR maps of sample G5-1 (R_o = 1.32%) at different time periods of exposure.

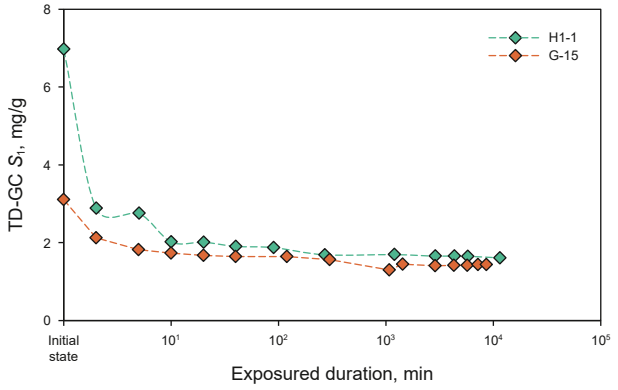


Fig. 5. Variation of oil content detected by TD-GC.

representing a loss rate of 37.34%. After 7 days, the S_1 of the pulverized sample was 1.14 mg/g, with 51.07% of the crude oil evaporated (Fig. 6(a), (c)). For sample G5-1, the initial S_1 was 1.86 mg/g. The oil content exhibited a fluctuating downward trend, primarily attributed to the sample's heterogeneity. After 7 days, the S_1 was 1.20 mg/g, corresponding to a loss rate of 35.48% (Fig. 6(b) and (c)).

4.1.4. Comparison of oil contents detected by three methods

For sample H1-1, the initial oil content was determined by different methods. T_1-T_2 NMR showed an oil content of 13.36 mg/g, while TD-GC measured 6.97 mg/g, and Rock-Eval pyrolysis recorded 2.33 mg/g. In the TD-GC analysis, the block sample was grinded to powder with 20–60 mesh. Crushing exposes numerous previously confined and even closed pores to the atmosphere, thereby enhancing evaporation of light hydrocarbons and resulting in a 47.83% reduction in oil content. The Rock-Eval pyrolysis required further crushing to 60–80 mesh. After the pulverized sample was placed in the crucible, it was held in the instrument for about 5 min before entering the pyrolysis furnace, which further exacerbated hydrocarbon loss (Li et al., 2022a; Wang et al., 2022a). The combined effects of grinding and waiting period resulted in an 82.66% reduction in oil content. Similarly, for the sample G5-1, the oil contents obtained by T_1-T_2 NMR, TD-GC, and Rock-Eval pyrolysis were 7.01, 3.10, and 1.86 mg/g, respectively. In the TD-GC analysis, crushing resulted in a 55.78% reduction in oil content, while the crushing and waiting period in the Rock-Eval pyrolysis led to a 73.47% reduction.

T_1-T_2 NMR measurements are performed on intact bulk rock samples, whereas TD-GC and Rock-Eval analyses require the samples to be crushed into powder prior to testing. During the crushing process, pores—particularly restricted and originally closed pores—are newly exposed, resulting in rapid volatilization and loss of pore fluids, which can lead to an underestimation of oil content in subsequent measurements. In TD-GC experiments, the crushed samples are placed in a sealed system; although volatilization may occur, the released hydrocarbons are continuously transported by purge gas and captured in a cold trap for analysis. In contrast, Rock-Eval measurements are conducted under open-system conditions: samples are loaded into crucibles and

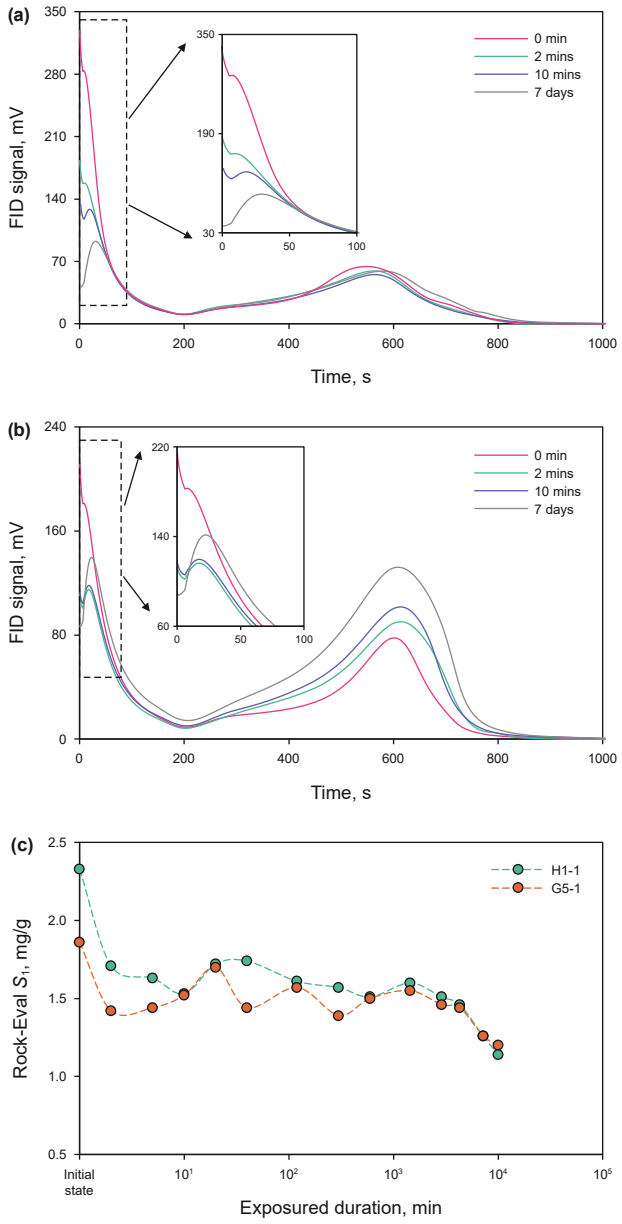


Fig. 6. Variation of oil content detected by Rock-Eval pyrolysis. **(a)** FID pyrograms of sample H1-1, **(b)** FID pyrograms of sample G5-1, **(c)** Variation of Rock-Eval S_1.

exposed to the atmosphere. Moreover, prior to the formal pyrolysis stage, the samples typically remain in the crucibles for approximately 5 min while the oven temperature increases to 300 °C, which further enhances hydrocarbon loss during this preheating interval.

As a result, for the same moderately to highly mature shale sample, NMR generally yields the highest apparent oil content, followed by TD-GC, whereas Rock-Eval produces the lowest values. Notably, the discrepancies among these three methods tend to become more pronounced with increasing thermal maturity. A more detailed comparison of the physical and chemical mechanisms governing oil-content detection by these methods in medium-to high-maturity shales can be found in previously published studies by our research group (Wang et al., 2022a; Li et al., 2022a).

4.2. Composition changes of retained hydrocarbons during exposure

TD-GC analysis was used to characterize composition changes of retained hydrocarbons during exposure. The TD-GC chromatograms of samples H1-1 and G5-1 at various exposed time were shown in Figs. 7 and 8, with *n*-alkane content also detailed in Fig. 9. The TD-GC analysis was conducted immediately after the frozen samples were crushed. In the initial state, distinct peaks of gaseous hydrocarbons were observed, with the thermally released hydrocarbons exhibiting a range of $nC_{1–23}$. For sample H1-1, the initial methane content was 0.57 mg/g. The contents of $nC_{1–5}$ and $nC_{6–14}$ were 2.17 mg/g and 1.75 mg/g, respectively, accounting for 48.20% and 38.77% of the total *n*-alkanes. After 2 min, the methane content dropped sharply to 0.03 mg/g. The $nC_{1–5}$ content decreased by 90.78% to 0.20 mg/g, while the $nC_{6–14}$ content dropped by 44.57% to 0.97 mg/g. After 10 min, the $nC_{6–14}$ content further decreases to 0.73 mg/g. As exposed time increased, the lighter hydrocarbons continued to evaporate. After 8 days, the concentration of the individual $nC_{1–8}$ compound drops to less than 0.01 mg/g, indicating that these compounds were almost entirely depleted. Meanwhile, the $nC_{6–14}$ content dropped to 0.49 mg/g. In addition, some heavy hydrocarbons were also lost, although at a lower rate. The initial $nC_{15–20}$ content was 0.50 mg/g. After 2 min, it decreased to 0.41 mg/g, and by 10 min, it further declined to 0.38 mg/g. Beyond this period, the $nC_{15–20}$ content stabilized, reaching 0.37 mg/g after 8 days (Fig. 9(a)).

The oil content of sample G5-1 is significantly lower than that of sample H1-1, primarily due to lower thermal maturity. Initially, the $nC_{1–5}$ content was 0.4370 mg/g, accounting for 25.05% of the total *n*-alkane content, while the $nC_{6–14}$ content was 0.8484 mg/g. After 2 min, the $nC_{1–5}$ content decreased by 94.76% to 0.0230 mg/g, and the $nC_{6–14}$ content dropped by 32.58% to 0.5720 mg/g. After 10 min, the $nC_{1–5}$ content further decreased to 0.0094 mg/g, indicating that gaseous hydrocarbons were nearly completely lost. By 6 days, the concentration of the individual $nC_{1–11}$ compound drops to less than 0.01 mg/g and the $nC_{6–14}$ content declined by 71.91% to 0.2383 mg/g. Additionally, the content of *n*-alkanes with carbon numbers below 12 was less than 0.01 mg/g, signifying that nC_{12-} compounds in the pulverized sample were almost entirely evaporative loss (Fig. 9(b)).

4.3. Model for hydrocarbon evaporation

Previous studies on the evaporation of bulk crude oil and petroleum products indicate that evaporation kinetics strongly depend on fluid composition. Mixtures composed of 5–7 components tend to follow a square-root-of-time relationship, whereas mixtures with more than ~7 components are better described by logarithmic or non-exponential functions (Fingas, 1997). Similarly, the mass loss of gasoline during evaporation has been shown to follow a logarithmic trend (Zhu et al., 2012), highlighting the increasing complexity of evaporation behavior with compositional diversity. In this study, the temporal evolution of oil content in three shale samples with different maturities exhibits distinct decay patterns. Samples B5-1 (R_o = 1.20%) and G5-1 (R_o = 1.32%) are well described by exponential decay models (Fig. 10(a) and (b)), whereas the higher-maturity sample H1-1 (R_o = 1.55%) follows a power-law decay trend (Fig. 10(c)). These differences are further clarified by analyzing their decay half-life characteristics.

For samples B5-1 and G5-1, the exponential decay implies a constant half-life, independent of the initial oil content. Based on the fitted models, the half-life is approximately 23.1 h for B5-1 and 6.93 h for G5-1. This behavior indicates that hydrocarbon loss

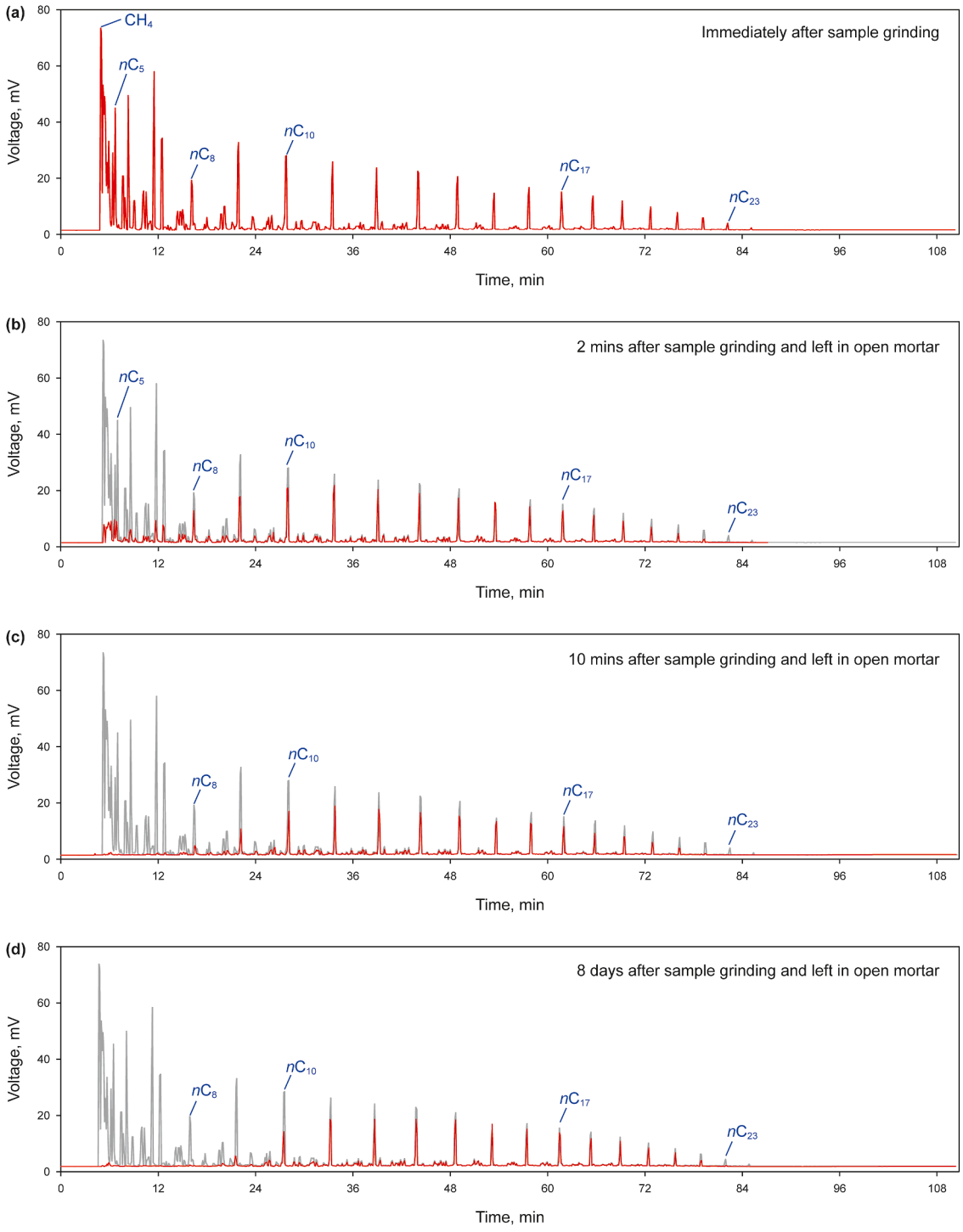


Fig. 7. TD-GC chromatograms showing the compositions of S_1-equivalent hydrocarbons thermally desorbed from sample H1-1.

proceeds at a rate proportional to the remaining oil content, reflecting a relatively uniform and single-timescale dissipation process. Such kinetics are consistent with shales of moderate maturity, where hydrocarbons are dominated by liquid components and pore connectivity remains limited, constraining diffusion pathways and maintaining a stable loss rate. In contrast, the oil content decay in sample H1-1 follows a power-law relationship, for which a fixed half-life cannot be strictly defined. Instead, the effective half-time increases progressively as oil content decreases, indicating a time-dependent attenuation process with a pronounced long-tail behavior. This suggests that hydrocarbon loss in H1-1 is governed not only by the instantaneous concentration but also by evolving transport constraints over time. The absence of a characteristic time scale reflects increasing resistance to hydrocarbon dissipation as readily mobile components are depleted.

The transition from exponential decay (B5-1 and G5-1) to power-law decay (H1-1) with increasing maturity implies a fundamental shift in the dominant hydrocarbon loss mechanism. At higher maturity, elevated proportions of light hydrocarbons,

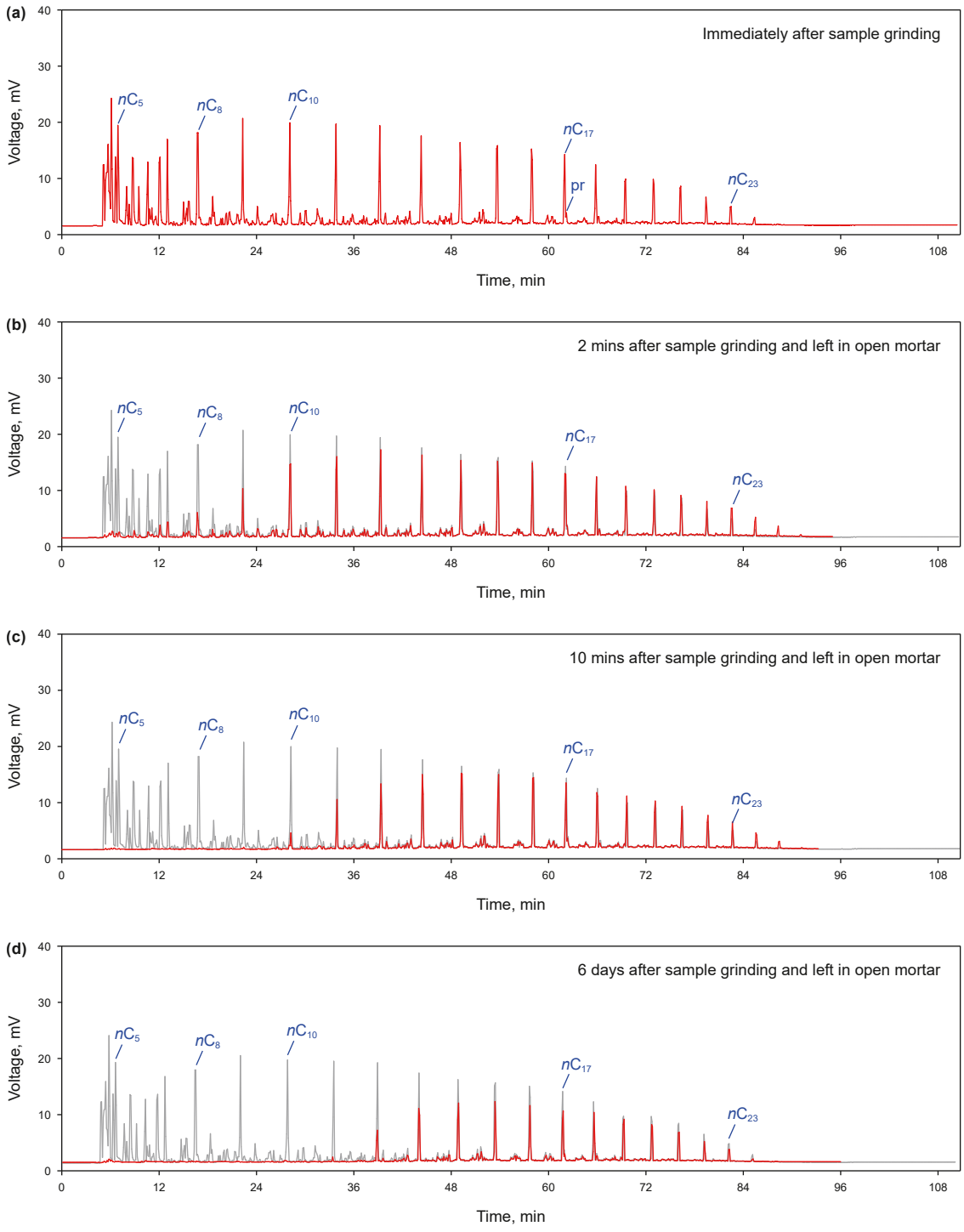


Fig. 8. TD-GC chromatograms showing the compositions of S_1-equivalent hydrocarbons thermally desorbed from sample G5-1.

enhanced molecular diversity, and more complex pore–throat architectures promote multi-scale diffusion and confinement effects, leading to non-exponential attenuation. Therefore, hydrocarbon evaporation in shale pores is controlled by a combination of fluid composition, maturity-dependent phase behavior, and pore structure heterogeneity, rather than by simple bulk evaporation kinetics alone. These controlling factors will be discussed in detail in the following sections.

T_1-T_2 NMR results show that both pore oil and pore water signals decrease with increasing storage time of pressure-retained cores, indicating that the loss of hydrocarbons and pore water occurs simultaneously. This synchronous attenuation reflects the progressive release of fluids from shale pores during storage rather than a single dominant process. In the present study, the analysis primarily focuses on the dissipation behavior of hydrocarbons, while pore water loss has not been quantitatively evaluated.

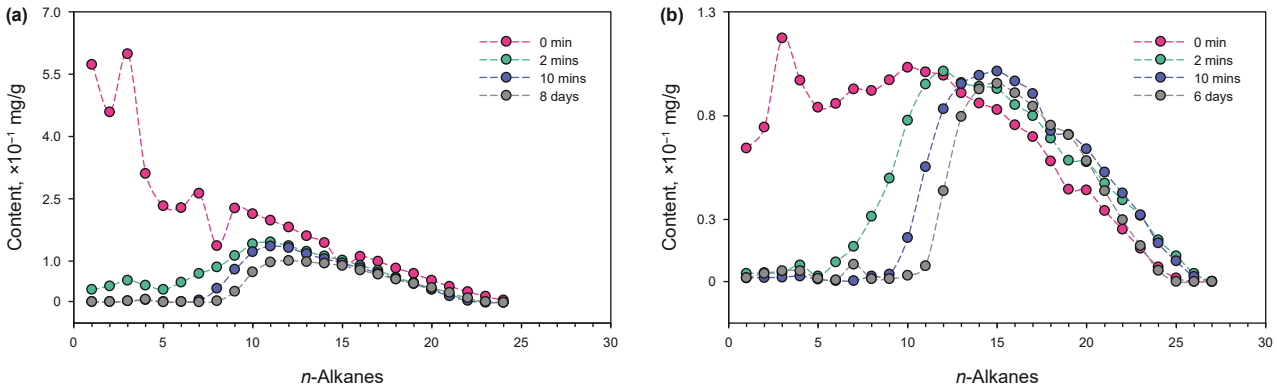


Fig. 9. Variation of normal alkanes content detected by TD-GC. **(a)** The normal alkanes content of sample H1-1 at different time periods of exposure, **(b)** The normal alkanes content of sample G5-1 at different time periods of exposure.

Existing studies suggest that pore water and hydrocarbon loss in shale are generally governed by different physical mechanisms and tend to proceed in parallel. Although variations in pore water content may locally affect pore-scale conditions, such as wettability or capillary pressure, their influence on hydrocarbon dissipation is considered secondary under the experimental conditions. Therefore, the observed concurrent decrease in oil and water signals is interpreted as parallel but not strongly coupled processes. Further investigation is required to clarify their potential interactions.

4.4. Factors affecting hydrocarbon evaporation

4.4.1. Thermal maturity

The oil contents of 51 cube samples (from 6 wells) in the exposed process were analyzed (Table S2). The higher the maturity, the greater the evaporative loss (Fig. 11). Thermal maturity controls evaporative loss of light hydrocarbons. The effect of thermal maturity on the evaporative loss of light hydrocarbons in medium-to high-maturity shale is reflected in two key aspects: its control over crude oil composition and pore structure. For Mbr 1 of the Qingshankou Fm in Gulong Sag, higher thermal maturity leads to greater degree pyrolysis for post-oil bitumen and retained oil, resulting in an increased proportion of light hydrocarbons in the shale interval. Although there are compositional differences between produced oil and in situ shale oil, the general trend reflects the effect of maturity on shale oil composition. When the thermal maturity of Mbr 1 of the Qingshankou Fm exceeds about 1.3%, the proportion of saturated hydrocarbons in the produced oil approaches 90%, indicating a significant increment of light hydrocarbons (Fig. S2(a)). The color of the produced oil can also intuitively illustrate the proportion of aliphatic hydrocarbons. The oil produced by H1 well is light yellow, while the oil produced by G5 well is bronze orange (Fig. S2(b)). Light hydrocarbons, characterized by smaller molecular sizes and weaker interactions with pore walls, are more prone to flow, diffuse and evaporate. As their proportion increases with higher maturity, the evaporative loss of light hydrocarbons becomes more significant.

The shale interval in the core area of the Gulong Sag has reached high thermal maturity stage (R_o > 1.2%). Retained oil and post-oil bitumen distributed between clay minerals and detrital particles have undergone extensive pyrolysis, leading to the formation of micro-nano pores (Wang et al., 2022b; Yan et al., 2024). The micropores in high maturity shale serve as storage spaces for in situ shale oil, while the nanopores act as connecting micropores, creating pathways for flow and diffusion of the light hydrocarbons. With increasing thermal maturity, pore volume provided by micropores and the proportion of connected pores improve, resulting in a higher loss ratio of light hydrocarbons.

4.4.2. Minerals and organic matter

The shale interval of Mbr 1 of Qingshankou Fm in the Gulong Sag primarily consists of clay minerals (mainly illite and illite-smectite mixed layers, with minor chlorite), quartz, and feldspar, with localized enrichment in carbonate minerals such as calcite and dolomite. Experimental analysis and molecular simulation technology indicate that different minerals exhibit varying adsorption capacities (Li et al., 2016, 2023; Yang et al., 2020; Cao et al., 2021). Kerogen has the strongest adsorption capacity for hydrocarbons in shale, followed by illite and illite-smectite mixed layers.

We took samples from target interval of G8 well (R_o = 1.45%–1.48%) as examples, the loss of light hydrocarbons was compared between shale and argillaceous siltstone. The results reveal a higher loss ratio in shale than in argillaceous siltstone (sample G8-093 and sample G8-189). Interestingly, the loss ratio does not show a clear relationship with clay mineral content (Fig. 12(a)) or organic matter content (Fig. 12(b)). To investigate this phenomenon further, nitrogen adsorption analysis was conducted to determine the nanopores size distribution. The results indicate that argillaceous siltstone has less well-developed pores with diameters under 100 nm compared to shale. The average pore volume for shale samples is 0.0528 cm^3/g, significantly higher than the 0.0187 cm^3/g for argillaceous siltstone samples (Fig. S3). The nanopores in shale act as connected path for micropores. In contrast, the nanopores in argillaceous siltstone are poor, resulting in limited connectivity and a lack of flow channels, which explains lower loss ratio of light hydrocarbons. Shale, with well-developed nanopores, exhibits superior pore connectivity, allowing fluids to diffuse and evaporate rapidly. In the high maturity stage, the adsorption capacity of organic matter decreases with increasing maturity, leading to minimal adsorption by organic matter and minerals (Li et al., 2023). This indicates that the impact of adsorption on the loss of light hydrocarbons is negligible. Based on the above analysis, it is concluded that for high maturity pure shale, the mineral composition primarily influences the evaporative loss of light hydrocarbons by altering the pore structure.

4.4.3. Physical state of sample

To investigate the influence of physical state (block or powder) on the evaporation of light hydrocarbons, intensive sampling was performed in B5 well to obtain 24 full-closure core samples. Each sample was divided into three parts for different analyses. The first part underwent T_1-T_2 NMR without crushing. The second part was

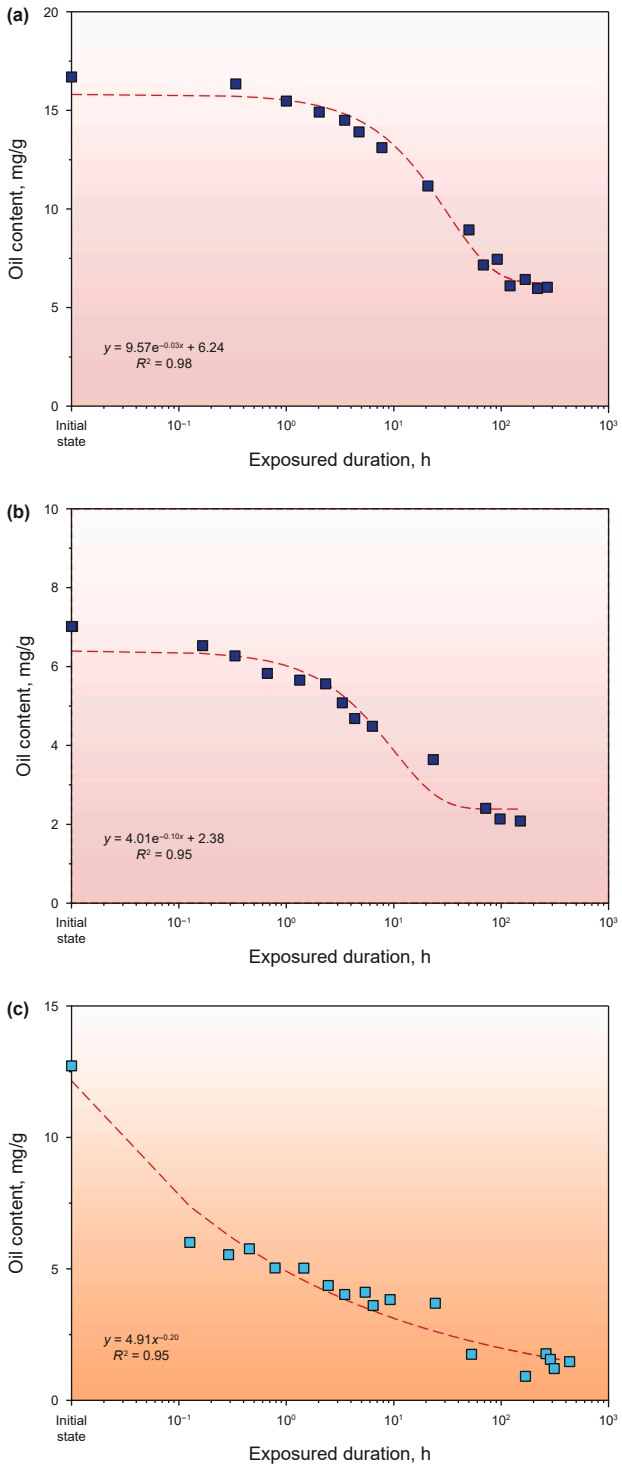


Fig. 10. Plots showing oil content measured by T_1-T_2 NMR with increasing exposure duration. **(a)** Sample B5-1, R_o = 1.20%, **(b)** Sample G5-1, R_o = 1.32%, **(c)** Sample H1-1, R_o = 1.55%.

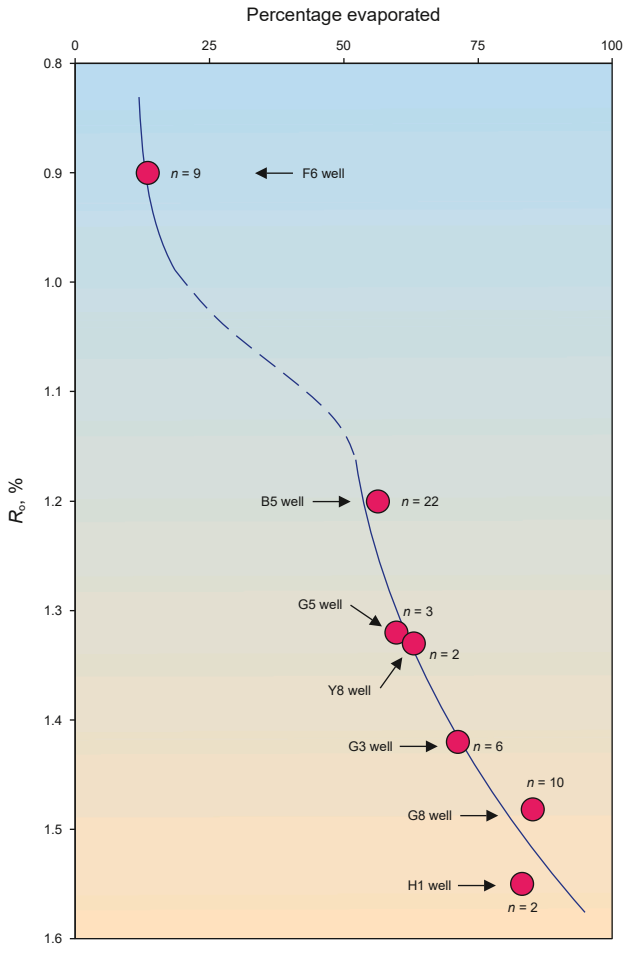


Fig. 11. Plot showing the percentage of evaporated light hydrocarbons with increasing thermal maturity. "*n*" refers to the number of samples used.

quickly crushed to 20–60 mesh for TD-GC analysis, while the third part was crushed to 60–80 mesh for Rock-Eval pyrolysis (Wang et al., 2022a).

The oil content measured by TD-GC was approximately 75% of that determined by T_1-T_2 NMR, indicating that about 25% of hydrocarbons were lost during crushing. Similarly, the oil content obtained from Rock-Eval was 78% of that from TD-GC, attributed to light hydrocarbons loss during the approximately 5-min waiting period before the crushed sample entered the pyrolysis furnace. The crushing process opens previously sealed pores, including confined and closed pores, exposing the hydrocarbons to air. To further assess this effect, long-stored block core sample (R_o = 1.55%) from Mbr 1 of the Qingshankou Fm were crushed into two parts. One was immediately analyzed using TD-GC, while the other was left in the laboratory for 15 days before testing. Comparisons revealed a significant reduction in residual hydrocarbons content, particularly nC_{11-14} compounds, which decreased by an average of 66.45% (Fig. S4). This confirms that crushing increases the exposure of heavier normal alkanes to air, intensifying hydrocarbon loss over time.

4.4.4. Storage conditions

A pressure-retained core sample (R_o = 1.46%, Mbr 2 of Qingshankou Fm, G8 well) was divided into three parts and exposed under different conditions: laboratory condition (about 22 °C, 55% relative humidity), desiccator (below 20% relative humidity), and oven (50 °C). The mass of each part is between 16 and 20 g. T_1-T_2 NMR analysis was conducted at various exposure times to determine the oil content. The oil content of the samples stored in the oven and the desiccator began to fluctuate slightly, eventually declining to 1.37 mg/g after 9 h and 72 h respectively. In contrast, the oil content of the samples stored in the laboratory condition showed a continuous decrease over 240 h (Fig. 13). Under low-humidity conditions, the total-pressure change induced by the removal of water vapor is relatively small (≈1.1% when relative humidity decreases from ~55%

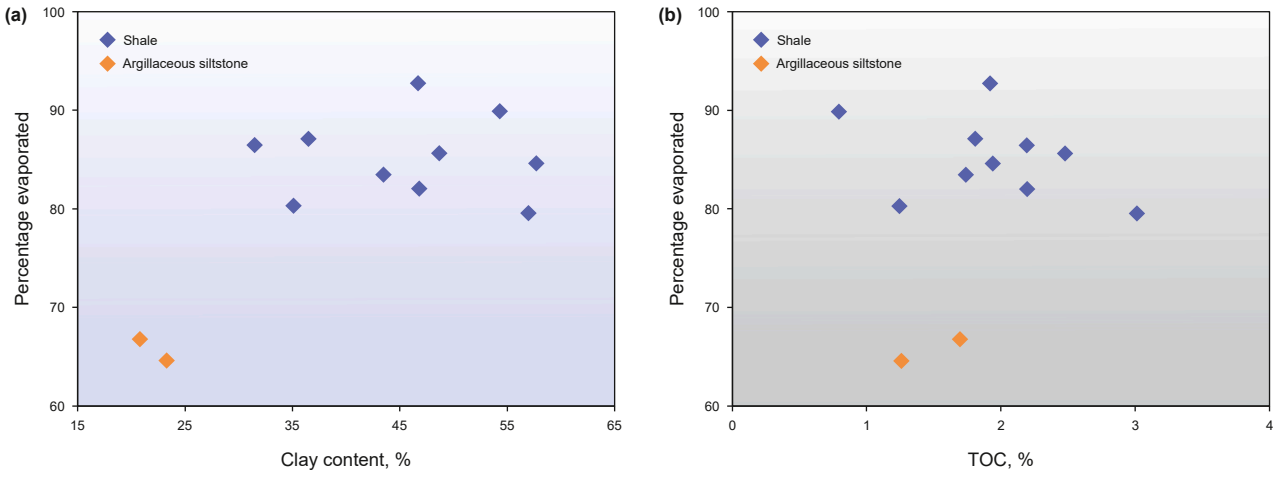


Fig. 12. Plots showing the percentage of evaporated light hydrocarbons with **(a)** clay content and **(b)** total organic carbon (TOC).

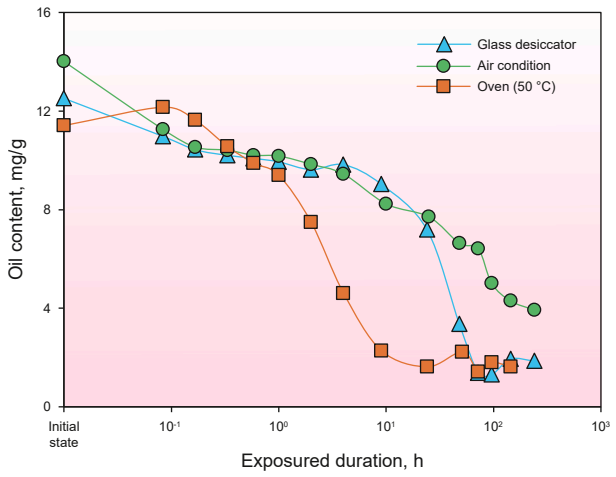


Fig. 13. Variation of oil content detected by T_1-T_2 NMR. The pressure-retained core samples were exposed under laboratory conditions, in a desiccator, and in an oven.

to <20% at ~25 °C). Therefore, the observed enhancement of oil loss is more reasonably attributed to changes in the partial-pressure driving force and mass-transfer resistance, and potentially to reduced pore-water occupancy or water-film effects that alleviate pore/throat blockage and facilitate hydrocarbon diffusion within shale nanopores (Tan et al., 2021). Nevertheless, the relative contributions and coupling mechanisms of these processes are not yet fully constrained and warrant further experimental and theoretical investigation.

A comparison of the experimental results revealed that the storage conditions, specifically temperature and humidity, significantly influence the loss rate of light hydrocarbons in shale. Higher temperatures increase molecular activity, accelerating the evaporation of light hydrocarbons. Similarly, lower humidity reduces the water vapor content in the air, preventing saturation and enhancing capacity to absorb volatile compounds. Additionally, under low-humidity conditions, a significant pressure gradient arises between the vapor pressure of light hydrocarbons in the shale and the surrounding air. The gradient promotes the evaporative loss of light hydrocarbons from the shale pore into the air.

5. Conclusions

Building upon the preceding analyses, this study synthesizes and further refines the experimental and analytical results to establish a systematic quantitative framework for evaluating evaporative losses of light hydrocarbons in medium-to high-maturity shale. By integrating variations in light hydrocarbon content with their compositional evolution during evaporation, this work elucidates the primary controls governing light hydrocarbon dissipation. Consequently, the results provide improved quantitative constraints for more accurate shale oil content evaluation and offer deeper insights into the occurrence characteristics and phase behavior of shale oil.

(1) Pressure-retained core samples are the most effective method for obtaining in situ oil content and composition, making them ideal for research on the evaporative loss of light hydrocarbons for high maturity shale. T_1-T_2 NMR analysis was employed to quantify the oil content during exposure, while TD-GC analysis was used to determine the composition of the retained hydrocarbons in shale.

(2) The evaporation of oil content in higher-maturity samples ($R_o \geq$ ~1.45%) was best described by a power-law decay, whereas an exponential decay provided a better fit for samples with lower thermal maturity (R_o = ~1.20%–~1.45%). The oil content measured by T_1-T_2 NMR was the highest, followed by TD-GC, which is attributed to the different physical state of samples used in each experiment (e.g., block, powder with varying mesh sizes). During the exposure of the pulverized sample, nearly all light hydrocarbon compounds (nC_{1-9}) in the shale were lost, and the heavier normal alkanes (nC_{10-20}) also experienced partial evaporation. The evaporation of heavier hydrocarbons was more pronounced in higher maturity samples. When evaluating oil content and determining the retained hydrocarbon composition in long-stored samples or medium-to high-maturity samples from conventional coring, it is crucial to account for the loss of light hydrocarbons.

(3) Thermal maturity plays a controlling role in the loss of light hydrocarbons, influencing both the oil composition and the pore structure. As maturity increases, the proportion of light hydrocarbons in oil rises, and the pore volume provided by

micropores increases, enhancing pore connectivity and accelerating the loss of light hydrocarbons. In the shale interval of Mbr 1 from the Qingshankou Fm in the Gulong Sag, mineralogical changes lead to alterations in pore structure, which, in turn, influence the loss of light hydrocarbons. A larger contact area between the sample and the air facilitates the loss of light hydrocarbons, with crushing further accelerating evaporation. Additionally, the storage conditions—specifically temperature and humidity—also influence hydrocarbon loss. Higher temperatures and lower humidity promote the evaporative loss of light hydrocarbons in shale samples.

The established restoration chart for light hydrocarbon content provides a practical tool for estimating in situ shale oil content from conventional core samples, which is particularly valuable for intervals where pressure-retained or sealed cores are unavailable. By comparing oil contents obtained from nuclear magnetic resonance (NMR), TD-GC, and Rock-Eval analyses, this study offers practical guidance for selecting appropriate evaluation methods under different sampling and preservation conditions. Moreover, the characterization of light hydrocarbon dispersion processes contributes to an improved understanding of fluid occurrence states and distribution within shale pore systems. Future research could focus on several key areas: the partial evaporation between normal alkanes and isoalkanes, carbon isotope fractionation, and the loss of pore water during the exposure of high maturity shale. Additionally, investigating the evaporative kinetics of individual *n*-alkanes compound—from pores to the sample surface and into the air—warrants further attention. While preliminary analyses have explored the effects of oil composition, pore structure, mineral composition, and organic carbon matter on hydrocarbon evaporation, more comprehensive and quantitative models are needed to achieve a deeper understanding of evaporative processes.

CRediT authorship contribution statement

Ming Li: Writing – original draft, Methodology, Investigation, Formal analysis, Conceptualization. **Yan Wu:** Data curation, Writing – review & editing. **Li Fu:** Validation, Resources, Methodology. **Min Wang:** Writing – review & editing, Supervision, Methodology. **Xue Wang:** Resources, Formal analysis. **Jin-Bu Li:** Writing – review & editing, Methodology, Investigation, Conceptualization. **Liang Xu:** Visualization, Formal analysis, Data curation. **Yong-He Sun:** Writing – review & editing. **Xin-Bin Zhao:** Visualization, Formal analysis. **Shang-De Dong:** Visualization, Investigation.

Declaration of competing interests

The authors declare that they have no known competing financial interests or personal relationships that could have appeared to influence the work reported in this paper.

Acknowledgements

The study was financially funded by the National Natural Science Foundation of China (No. 42473064, No. 42472190), the Project of Chongqing Talent Innovation Leading Talent for Education Field (No. 0255-19230101042), Shandong Province Postdoctoral Innovation Project (No. SDCX-ZG-202302009) and the Research Foundation of Chongqing University of Science and Technology (No. ckrc20241206).

Supplementary Information

Supplementary Information to this article can be found online at https://doi.org/10.1016/j.petsci.2026.05.010.

References

American Petroleum Institute, 1998. Recommended Practices for Core Analysis. API Publishing Services, Washington, USA.

Beti, D.R., Panja, P., Jiang, C., Milovic, M., Robinson, R., Ring, T.A., Levey, R., 2020. Change in hydrocarbon composition in rock samples as a function of time: a thermodynamic evaporation model. J. Nat. Gas Sci. Eng. 77, 103238. https://doi.org/10.1016/j.jngse.2020.103238.

Cañipa-Morales, N.K., Galán-Vidal, C.A., Guzmán-Vega, M.A., Jarvie, D.M., 2003. Effect of evaporation on C_7 light hydrocarbon parameters. Org. Geochem. 34 (6), 813–826. https://doi.org/10.1016/S0146-6380(03)00002-0.

Cao, Z., Jiang, H., Zeng, J., Saibi, H., Lu, T., Xie, X., Zhang, Y., Zhou, G., Wu, K., Guo, J., 2021. Nanoscale liquid hydrocarbon adsorption on clay minerals: a molecular dynamics simulation of shale oils. Chem. Eng. J. 420, 127578. https://doi.org/10.1016/j.cej.2020.127578.

Chen, J., Pang, X., Pang, H., Chen, Z., Jiang, C., 2018. Hydrocarbon evaporative loss evaluation of lacustrine shale oil based on mass balance method: permian Lucaogou formation in Jimusaer depression, Junggar Basin. Mar. Petrol. Geol. 91, 422–431. https://doi.org/10.1016/j.marpetgeo.2018.01.021.

Cooles, G.P., Mackenzie, A.S., Quigley, T.M., 1986. Calculation of petroleum masses generated and expelled from source rocks. Org. Geochem. 10, 235–245. https://doi.org/10.1016/0146-6380(86)90026-4.

Fingas, M.F., 1995. A literature review of the physics and predictive modelling of oil spill evaporation. J. Hazard. Mater. 42 (2), 157–175. https://doi.org/10.1016/0304-3894(95)00013-K.

Fingas, M.F., 1997. Studies on the evaporation of crude oil and petroleum products: I. the relationship between evaporation rate and time. J. Hazard. Mater. 56 (3), 227–236. https://doi.org/10.1016/S0304-3894(97)00050-2.

Fingas, M.F., 1998. Studies on the evaporation of crude oil and petroleum products II. Boundary layer regulation. J. Hazard. Mater. 57 (1), 41–58. https://doi.org/10.1016/S0304-3894(97)00051-4.

Fleury, M., Romero-Sarmiento, M., 2016. Characterization of shales using T_1-T_2 NMR maps. J. Pet. Sci. Eng. 137, 55–62. https://doi.org/10.1016/j.petrol.2015.11.006.

Guo, X., Wang, E., Ma, X., Li, M., Qian, M., Cao, T., Li, Z., Chu, J., 2025. Lacustrine shale oil systems in China: advances in characterization methods and resource accumulation models. Earth Sci. Rev. 270, 105256. https://doi.org/10.1016/j.earscirev.2025.105256.

He, W., 2023. Preliminary study on nanopores, nanofissures, and in situ accumulation of Gulong shale oil. Earth Sci. Front. 30 (1), 156–173. https://doi.org/10.13745/j.esf.sf.2022.8.32 (in Chinese).

Hu, S., Bai, B., Tao, S., Bian, C., Zhang, T., Chen, Y., Liang, X., Wang, L., Zhu, R., Jia, J., Pan, Z., Li, S., Liu, Y., 2022. Heterogeneous geological conditions and differential enrichment of medium and high maturity continental shale oil in China. Petrol. Explor. Dev. 49 (2), 257–271. https://doi.org/10.1016/S1876-3804(22)60022-3.

He, W., Meng, Q., Feng, Z., Zhang, J., Wang, R., 2022. In-situ accumulation theory and exploration & development practice of Gulong shale oil in Songliao Basin. Acta Pet. Sin. 43 (1), 1–14. https://doi.org/10.7623/syxb202201001 (in Chinese).

Jarvie, D., 2014. Components and processes affecting producibility and commerciality of shale resource systems. Geol. Acta 12, 307–325. https://doi.org/10.1344/GeologicaActa2014.12.4.3.

Jiang, C., Chen, Z., Mort, A., Milovic, M., Robinson, R., Stewart, R., Lavoie, D., 2016. Hydrocarbon evaporative loss from shale core samples as revealed by Rock-Eval and thermal desorption-gas chromatography analysis: its geochemical and geological implications. Mar. Petrol. Geol. 70, 294–303. https://doi.org/10.1016/j.marpetgeo.2015.11.021.

Jiang, Q., Li, M., Qian, M., Bao, Y., Liu, P., Tao, G., Ma, X., Li, Z., Cao, T., Wu, S., 2019. Experimental procedures of well-site geological evaluation for shale oil and related technological progress. Oil Gas Geol. 40 (3), 571–582. https://doi.org/10.11743/ogg20190312 (in Chinese).

Li, J., Huang, W., Lu, S., Wang, M., Chen, G., Tian, W., Guo, Z., 2018. Nuclear magnetic resonance T_1-T_2 map division method for hydrogen-bearing components in continental shale. Energy Fuels. 32 (9), 9043–9054. https://doi.org/10.1021/acs.energyfuels.8b01541.

Li, J., Jiang, C., Wang, M., Xu, L., Li, M., Yu, C., Wu, Y., Lu, S., 2022a. Determination of in situ hydrocarbon contents in shale oil plays. Part 1: is routine Rock–Eval analysis reliable for quantifying the hydrocarbon contents of preserved shale cores? Org. Geochem. 170, 104449. https://doi.org/10.1016/j.orggeochem.2022.104449.

Li, J., Lu, S., Chen, G., Wang, M., Tian, S., Guo, Z., 2019a. A new method for measuring shale porosity with low-field nuclear magnetic resonance considering non-fluid signals. Mar. Petrol. Geol. 102, 535–543. https://doi.org/10.1016/j.marpetgeo.2019.01.013.

Li, J., Lu, S., Jiang, C., Wang, M., Chen, Z., Chen, G., Li, J., Lu, S., 2019b. Characterization of shale pore size distribution by NMR considering the influence of shale skeleton signals. Energy Fuels. 33 (7), 6361–6372. https://doi.org/10.1021/acs.energyfuels.9b01317.

Li, J., Wang, M., Fei, J., Xu, L., Shao, H., Li, M., Tian, W., Lu, S., 2022b. Determination of in situ hydrocarbon contents in shale oil plays. Part 2: Two-dimensional nuclear magnetic resonance (2D NMR) as a potential approach to characterize preserved cores. Mar. Petrol. Geol. 145, 105890. https://doi.org/10.1016/j.marpetgeo.2022.105890.

Li, J., Wang, M., Jia, W., 2024b. A modified surface to volume (SVR) method to calculate nuclear magnetic resonance (NMR) surface relaxivity: theory and a case study in shale reservoirs. Mar. Petrol. Geol. 170, 107159. https://doi.org/10.1016/j.marpetgeo.2024.107159.

Li, J., Wang, M., Lu, S., Liu, L., Li, M., Zhang, Y., Wang, X., Zhao, X., Zhang, J., Zhao, Y., 2023. Quantitative evaluation model of shale oil adsorption: a case study of the first member of Cretaceous Qingshankou Formation in northern Songliao Basin, NE China. Petrol. Explor. Dev. 50 (5), 1137–1150. https://doi.org/10.1016/S1876-3804(23)60454-9.

Li, M., Wang, M., Zhang, L., Wang, Q., Wang, X., Li, X., Deng, Z., Dong, S., 2024c. Understanding pore space and oil content of liquid-rich shale in the southern Bohai Sea, China. Geoenergy Sci. Eng. 233, 212552. https://doi.org/10.1016/j.geoen.2023.212552.

Li, M., Wang, M., Zhao, C., Zhang, J., Liu, Z., Zhao, X., Li, J., Chen, J., 2024a. Compositional differences of near-critical petroleum from closed pores to wellhead in Gulong shale oil play, Songliao Basin, NE China. Mar. Petrol. Geol. 167, 106968. https://doi.org/10.1016/j.marpetgeo.2024.106968.

Li, Y., Xiong, Y., Chen, Y., Tang, Y., 2014. The effect of evaporation on the concentration and distribution of diamondoids in oils. Org. Geochem. 69, 88–97. https://doi.org/10.1016/j.orggeochem.2014.02.007.

Li, Z., Zou, Y., Xu, X., Sun, J., Li, M., Peng, P.A., 2016. Adsorption of mudstone source rock for shale oil—experiments, model and a case study. Org. Geochem. 92, 55–62. https://doi.org/10.1016/j.orggeochem.2015.12.009.

Liu, B., Bai, L., Chi, Y., Jia, R., Fu, X., Yang, L., 2019. Geochemical characterization and quantitative evaluation of shale oil reservoir by two-dimensional nuclear magnetic resonance and quantitative grain fluorescence on extract: a case study from the Qingshankou formation in Southern Songliao Basin, northeast China. Mar. Petrol. Geol. 109, 561–573. https://doi.org/10.1016/j.marpetgeo.2019.06.046.

Liu, B., Liu, L., Fu, J., Lin, T., He, J., Liu, X., Liu, Y., Fu, X., 2023. The songliao super Basin in northeastern China. AAPG Bull. 107 (8), 1257–1297. https://doi.org/10.1306/02242321181.

Liu, W., Jia, W., Wang, Q., Chen, J., Li, J., Peng, P.A., 2024. Influencing factors of hydrogen isotopic fractionation of light hydrocarbons during evaporation and implications. Org. Geochem. 198, 104894. https://doi.org/10.1016/j.orggeochem.2024.104894.

Mango, F.D., 1997. The light hydrocarbons in petroleum: a critical review. Org. Geochem. 26 (7–8), 417–440. https://doi.org/10.1016/S0146-6380(97)00031-4.

Mukhametdinova, A., Habina-Skrzyniarz, I., Kazak, A., Krzyżak, A., 2021. NMR relaxometry interpretation of source rock liquid saturation — a holistic approach. Mar. Petrol. Geol. 132, 105165. https://doi.org/10.1016/j.marpetgeo.2021.105165.

Okamoto, K., Watanabe, N., Hagimoto, Y., Miwa, K., Ohtani, H., 2010. Evaporation characteristics of multi-component liquid. J. Loss Prev. Process. Ind. 23 (1), 89–97. https://doi.org/10.1016/j.jlp.2009.06.004.

Qian, M., Li, M., Jiang, Q., Li, Z., Tao, G., Bao, Y., 2022. Evaluation of evaporative loss of hydrocarbon in shale samples and its geological implications. Petrol. Geol. Exp. 44 (3), 497–504. https://doi.org/10.11781/sysydz202203497 (in Chinese).

Romero-Sarmiento, M., Pillot, D., Letort, G., Lamoureux-Var, V., Beaumont, V., Huc, A., Garcia, B., 2016a. New rock-eval method for characterization of unconventional shale resource systems. Oil Gas Sci. Technol. 71 (3), 37. https://doi.org/10.2516/ogst/2015007.

Romero-Sarmiento, M., Euzen, T., Rohais, S., Jiang, C., Littke, R., 2016b. Artificial thermal maturation of source rocks at different thermal maturity levels: application to the Triassic Montney and Doig formations in the Western Canada sedimentary basin. Org. Geochem. 97, 148–162. https://doi.org/10.1016/j.orggeochem.2016.05.002.

Romero-Sarmiento, M., 2019. A quick analytical approach to estimate both free versus sorbed hydrocarbon contents in liquid-rich source rocks. AAPG Bull. 103 (9), 2031–2043. https://doi.org/10.1306/02151918152.

Song, Y., Kausik, R., 2019. NMR application in unconventional shale reservoirs – a new porous media research frontier. Prog. Nucl. Magn. Reson. Spectrosc. 112–113, 17–33. https://doi.org/10.1016/j.pnmrs.2019.03.002.

Sun, L., Cui, B., Zhu, R., Wang, R., Feng, Z., Li, B., Zhang, J., Gao, B., Wang, Q., Zeng, H., Liao, Y., Jiang, H., 2023. Shale oil enrichment evaluation and production law in Gulong Sag, Songliao Basin, NE China. Petrol. Explor. Dev. 50 (3), 505–519. https://doi.org/10.1016/S1876-3804(23)60406-9.

Sun, L., Liu, H., He, W., Li, G., Zhang, S., Zhu, R., Jin, X., Meng, S., Jiang, H., 2021. An analysis of major scientific problems and research paths of Gulong shale oil in Daqing Oilfield, NE China. Petrol. Explor. Dev. 48 (3), 527–540. https://doi.org/10.1016/S1876-3804(21)60043-5.

Sun, X., Wan, Y., Liu, Z., Dong, Z., Xiao, Q., 2013. Effects of natural evaporation on C5-C8 light hydrocarbon in dicators: evidence from experimental results in the labratory. Acta Pet. Sin. 34 (6), 1060–1069. https://doi.org/10.7623/syxb201306004 (in Chinese).

Tan, Y., Zhang, S., Tang, S., Cui, G., Ma, Y., Sun, M., Pan, Z., 2021. Impact of water saturation on gas permeability in shale: experimental and modelling. J. Nat. Gas Sci. Eng. 95, 104062. https://doi.org/10.1016/j.jngse.2021.104062.

Wang, E., Feng, Y., Guo, T., Li, M., 2022. Oil content and resource quality evaluation methods for lacustrine shale: a review and a novel three-dimensional quality evaluation model. Earth Sci. Rev. 232, 104134. https://doi.org/10.1016/j.earscirev.2022.104134.

Wang, M., Li, M., Li, J., Xu, L., Shao, H., Yu, C., Li, T., 2022a. Comparative analysis of test methods for shale oil content. Acta Pet. Sin. 43 (12), 1758–1769. https://doi.org/10.7623/syxb202212007 (in Chinese).

Wang, M., Tian, S., Chen, G., Xue, H., Huang, A., Wang, W., 2014. Correction method of light hydrocarbons losing and heavy hydrocarbon handling for residual hydrocarbon (S_1) from Shale. Acta Geol. Sin. Engl. Ed. 88 (6), 1792–1797. https://doi.org/10.1111/1755-6724.12345.

Wang, X., Cui, B., Feng, Z., Shao, H., Huo, Q., Zhang, B., Gao, B., Zeng, H., 2023. In-situ hydrocarbon formation and accumulation mechanisms of micro- and nano-scale pore-fracture in Gulong shale, Songliao Basin, NE China. Petrol. Explor. Dev. 50 (6), 1269–1281. https://doi.org/10.1016/S1876-3804(24)60465-9.

Wang, X., Wang, M., Li, J., Shao, H., Deng, Z., Wu, Y., 2022b. Thermal maturity: the controlling factor of wettability, pore structure, and oil content in the lacustrine Qingshankou shale, Songliao Basin. J. Pet. Sci. Eng. 215, 110618. https://doi.org/10.1016/j.petrol.2022.110618.

Xiao, Q., Sun, Y., Zhang, Y., Chai, P., 2012. Stable carbon isotope fractionation of individual light hydrocarbons in the C_6–C_8 range in crude oil as induced by natural evaporation: experimental results and geological implications. Org. Geochem. 50, 44–56. https://doi.org/10.1016/j.orggeochem.2012.06.003.

Yan, Y., Wang, M., Misch, D., Sachsenhofer, R.F., Wu, Y., Li, J., 2024. Mineral diagenesis in lacustrine organic-rich shales: evolution pathways and implications for reservoir characteristics. J. Asian Earth Sci. 236, 106026. https://doi.org/10.1016/j.jseaes.2024.106026.

Yang, Y., Liu, J., Yao, J., Kou, J., Li, Z., Wu, T., Zhang, K., Zhang, L., Sun, H., 2020. Adsorption behaviors of shale oil in kerogen slit by molecular simulation. Chem. Eng. J. 387, 124054. https://doi.org/10.1016/j.cej.2020.124054.

Zeng, H., Huo, Q., Wang, Y., Zhang, X., Fan, Q., Qiao, Y., 2021. A comparison of hydrocarbon loss between pyrolysis S_1 and crude oils: a case study of Qingshankou shale-oil system, Songliao Basin. In: 30th International Meeting on Organic Geochemistry. https://doi.org/10.3997/2214-4609.202134087.

Zhang, P., Lu, S., Li, J., Chang, X., 2020. 1D and 2D Nuclear magnetic resonance (NMR) relaxation behaviors of protons in clay, kerogen and oil-bearing shale rocks. Mar. Petrol. Geol. 114, 104210. https://doi.org/10.1016/j.marpetgeo.2019.104210.

Zhang, S., Wang, M., Zhu, X., Li, C., Cai, J., Yan, J., 2024. Oil saturation quantitative evaluation in lacustrine shale: novel insights from NMR T_1-T_2 and displacement experiments. Fuel 371. https://doi.org/10.1016/j.fuel.2024.132062.

Zhao, W., Bian, C., Li, Y., Zhang, J., He, K., Liu, W., Zhang, B., Lei, Z., Liu, C., Zhang, J., Guan, M., Liu, S., 2023b. Enrichment factors of movable hydrocarbons in lacustrine shale oil and exploration potential of shale oil in Gulong Sag, Songliao Basin, NE China. Petrol. Explor. Dev. 50 (3), 520–533. https://doi.org/10.1016/S1876-3804(23)60407-0.

Zhao, W., Hu, S., Hou, L., Yang, T., Li, X., Guo, B., Yang, Z., 2020. Types and resource potential of continental shale oil in China and its boundary with tight oil. Petrol. Explor. Dev. 47 (1), 1–11. https://doi.org/10.1016/S1876-3804(20)60001-5.

Zhao, W., Zhu, R., Liu, W., Bian, C., Wang, K., 2023a. Lacustrine medium-high maturity shale oil in onshore China: enrichment conditions and occurrence features. Earth Sci. Front. 30 (1), 116–127. https://doi.org/10.13745/j.esf.sf.2022.8.31 (in Chinese).

Zhu, L., Chen, J., Liu, Y., Geng, R., Yu, J., 2012. Experimental analysis of the evaporation process for gasoline. J. Loss Prev. Process. Ind. 25 (6), 916–922. https://doi.org/10.1016/j.jlp.2012.05.002.

Zhu, R., Zhang, L., Li, J., Liu, Q., Li, Z., Wang, R., Zhang, L., 2015. Quantitative evaluation of residual liquid hydrocarbons in shale. Acta Pet. Sin. 36 (1), 13–18. https://doi.org/10.7623/syxb201501002 (in Chinese).

Zhu, G., Wang, X., Zhang, J., Liu, Z., Bai, Y., Zhao, Y., Fu, X., Zeng, H., 2023. Enrichment conditions and favorable zones for exploration and development of continental shale oil in Songliao Basin. Acta Pet. Sin. 44 (1), 110–124. https://doi.org/10.7623/syxb202301007 (in Chinese).